Diverse surface signatures of stratospheric polar vortex anomalies

E. W. Kolstad[1], S. H. Lee[2], A. H. Butler[3], D. I. V. Domeisen[4], and C. O. Wulff[1]

[1] NORCE Norwegian Research Center, Bjerknes Center for Climate Research, Bergen, Norway.

[2] Department of Applied Physics and Applied Mathematics, Columbia University, New York, New York, USA.

[3] NOAA Chemical Sciences Laboratory, Boulder, Colorado, USA.

[4] University of Lausanne, Lausanne, Switzerland / ETH Zurich, Zurich, Switzerland

Corresponding author: Erik Kolstad (ekol@norceresearch.no)

Key Points:

- The broad spectrum of surface signatures of stratospheric polar vortex anomalies may be obscured by the small observational sample size.
- Observed Eurasian cold signature during weak vortex states could be artificially strong due to insufficient sampling.
- Over North America the main driver of winter temperature variability is ENSO, but the stratosphere can modulate ENSO teleconnections.

Abstract

The Arctic stratospheric polar vortex is an important driver of winter weather and climate variability and predictability in North America and Eurasia, with a downward influence that on average projects onto the North Atlantic Oscillation (NAO). While tropospheric circulation anomalies accompanying anomalous vortex states display substantial case-by-case variability, understanding the full diversity of the surface signatures requires larger sample sizes than those available from reanalyses. Here, we first show that a large ensemble of seasonal hindcasts realistically reproduces the observed average surface signatures for weak and strong vortex winters and produces sufficient spread for single ensemble members to be considered as alternative realizations. We then use the ensemble to analyze the diversity of surface signatures during the 25% weakest and strongest vortex winters. Over Eurasia, only one of three weak vortex clusters yields continent-wide cold conditions, suggesting that the observed Eurasian cold signature could be artificially strong due to insufficient sampling. For both weak and strong vortex cases, the canonical temperature pattern in Eurasia only clearly arises when North Atlantic sea surface temperatures exhibit the tripolar structure in-phase with the NAO. Over North America, while the main driver of interannual winter temperature variability is the El Niño–Southern Oscillation (ENSO), the stratosphere can modulate ENSO teleconnections, affecting temperature and circulation anomalies over North America and downstream. These findings confirm that anomalous vortex states are associated with a broad spectrum of surface climate anomalies on the seasonal scale, which may be obscured by the small observational sample size.

Plain Language Summary

The strength of the winds in the stratosphere over the Arctic provides useful information for seasonal forecasts of wintertime weather over Europe and North America. When we study these linkages, it is a challenge that we have few winters – only about 40 – with reliable observations from the stratosphere. Here we use a seasonal forecast model to generate a large collection of 3000 possible winters, and we use these to examine different patterns of surface temperature and sea level pressure for winters with the strongest and weakest winds in the polar stratosphere. Some real-world episodes have attracted wide attention, including recent cold winters linked to weak stratospheric winds, and there seems to be an anticipation that weak winds in the stratosphere are synonymous with cold weather in many regions. However, our results indicate that these expected surface signatures are in fact not particularly common. There are also scenarios when instead the opposite surface signature emerges. We find that it is not sufficient to know the state of the stratosphere; regional sea surface temperatures can either support or counteract the stratospheric influence on winter weather in any given year.

1 Introduction

During winter, when no sunlight reaches the polar regions, the air in the upper stratosphere is cold and dense. The resulting large-scale cyclonic system over the polar cap is surrounded by strong westerly winds, forming the stratospheric polar vortex. It is now well-known that the strength of the vortex is related to the atmospheric circulation near the surface (e.g., Kidston et al., 2015). A little more than every other winter on average, this cyclonic circulation is significantly disrupted: the westerly winds in the stratosphere rapidly decelerate and can reverse direction in an event known as a (major) Sudden Stratospheric Warming (SSW) (Baldwin et al., 2021). In the weeks to months following the onset of an SSW, the North Atlantic

Oscillation (NAO) – the pattern that explains the most variance in the large-scale circulation in the North Atlantic region (Ambaum et al., 2001) – is more often than not in a negative state (Hitchcock & Simpson, 2014; Afargan-Gerstman & Domeisen, 2020). Conversely, when the vortex is stronger than normal, the NAO is usually positive (Ambaum & Hoskins, 2002). This effect is also true for the closely related hemispheric-scale Northern Annular Mode (NAM), also referred to as the Arctic Oscillation (AO) (Baldwin & Dunkerton, 1999; Black & McDaniel, 2004).

Weather types associated with anomalous vortex states, such as blocking (Kautz et al., 2022) and/or negative NAO events (Charlton-Perez et al., 2018), affect renewable energy demand and production (van der Wiel et al., 2019). Hence, it is not surprising that the state of the vortex influences futures markets in the energy sector (Beerli et al., 2017). Discussions between the authors and energy traders have revealed that the expectation of cold weather related to SSWs can have a large influence on energy prices. In the UK, where the climate is significantly influenced by the NAO, the SSW on 5 January 2021 (Lee, 2021) was followed by clear spikes in the electricity auction prices. For example, Elexon UK, a British market regulator, wrote on 11 January 2021: 'System Prices reached or exceeded £1,000/MWh on seven occasions from 6 to 8 January due to cold weather brought on from the "Beast from the East 2".'[1] The colloquial term 'Beast from the East' refers to notably cold easterly winds; whilst it is not a new phrase[2], it gained popularity after an extreme European cold wave during February/March 2018 (Greening & Hodgson, 2019), following an SSW in mid-February (Lü et al., 2020).

Yet, while the average response is robust, the relationship between vortex strength and surface circulation is nuanced and case dependent. For example, only around two-thirds of SSWs are followed by a persistent negative NAO event, and less than a quarter of negative NAO events are preceded by an SSW (Domeisen, 2019). Departures from the most typical (or 'canonical') tropospheric response have been linked to various differences across SSW events, such as the evolution of the stratospheric flow and its rate and depth of downward propagation (Maycock & Hitchcock, 2015; Karpechko et al., 2017) and the state of the troposphere as the SSW unfolds (Garfinkel et al., 2013; White et al., 2019; Afargan-Gerstman & Domeisen, 2020). Moreover, the vortex has been shown to influence surface climate in more diverse ways than is revealed by considering solely the NAO (Beerli & Grams, 2019; Domeisen et al., 2020c), particularly over North America (Kretschmer et al., 2018; Cohen et al., 2021; Lee et al., 2022). There is also a complex relationship between the stratospheric vortex and tropical variability, including the Madden-Julian Oscillation (MJO) and El Niño-Southern Oscillation (ENSO), which can influence the state of the vortex through tropical-extratropical teleconnections (Barnes et al., 2019; Domeisen et al., 2019; Green & Furtado, 2019) and can also directly modulate the tropospheric response to the stratosphere (Jiménez-Esteve & Domeisen, 2020; Knight et al., 2021). Furthermore, tropospheric precursors to extreme stratospheric states, such as blocking, may induce systematic tropospheric temperature anomaly patterns before and during the onset of anomalous vortex states, independent of the downward propagation of the stratospheric vortex anomaly (e.g., Kolstad & Charlton-Perez, 2011).

We speculate that expectations of tropospheric responses to anomalous vortex states have been influenced by recent amplified manifestations of the 'canonical' response, such as the cold winter in Northern Europe in 2010 before, during and after an SSW (Cohen et al., 2010), the

[1] https://www.elexon.co.uk/article/system-prices-spike-due-to-beast-from-the-east-ii/
[2] https://blog.metoffice.gov.uk/2012/12/07/the-meteorology-behind-the-beast-from-the-east/

"Beast from the East" episodes in 2018 and 2021 (both occurring after SSWs), and the strong vortex winter of 2020 (Lawrence et al., 2020; Rupp et al., 2022), which was associated with record heat over northern Eurasia (Schubert et al., 2022). These events have also coincided with increased appreciation of the impact of stratospheric variability and our improved ability to represent it within models over the last decade (Domeisen et al., 2020a). It is therefore important to better understand and quantify the diversity in the relationship between vortex strength and surface climate, which is what we address herein.

While case studies and sensitivity experiments are essential for understanding the complexity of stratosphere–troposphere interactions, a ubiquitous challenge in climate prediction is that there are a limited number of years and events to study. For instance, after more frequent observations started in 1958 there have only been roughly six SSWs per decade (Butler et al., 2017). To deal with the limited sample size, Oehrlein et al. (2021) used a bootstrapping technique to explore the distribution of surface impacts of SSWs. A different approach is to leverage climate or forecast model ensemble simulations to obtain a larger sample size for climate variability studies (van den Brink et al., 2004, 2005; Breivik et al., 2013; Weaver et al., 2014; Chen & Kumar, 2017; Kent et al., 2017; Thompson et al., 2017; Kelder et al., 2020; Brunner & Slater, 2022). Closer to the issue at hand here, Wang et al. (2020) used seasonal forecast model data to estimate the chances of an SSW in the Southern Hemisphere, and Spaeth and Birner (2021) and Monnin et al. (2022) used sub-seasonal and seasonal forecast model data, respectively, to study SSWs.

Here we harness hindcasts and forecasts from the European Centre for Medium-range Weather Forecasts (ECMWF) seasonal prediction system SEAS5 (Johnson et al., 2019) to obtain 3000 'potential' winter seasons between 1981 and 2020, 75 times more than the 40 observed winters in the same period. We focus on the period from December to March (DJFM), as this period has the highest frequency of SSWs (Butler et al., 2017) and the largest vortex variability (Baldwin et al., 2003), and we study seasonal means to filter out the impacts of intraseasonal variations. First, we validate the model's representation of stratospheric vortex variability and its linkages between anomalous vortex states and surface variables by comparing with reanalysis. Then, we investigate the most common surface signatures of anomalous vortex states by means of a clustering algorithm based on temperature anomalies over land, studying Eurasia and North America separately. Our results highlight the wide diversity of surface signatures related to both strong and weak vortex states across the two continents on the seasonal scale. We conclude by discussing the results and their relevance for forecast interpretation.

2 Data and Methods

We use data from two sources, the ERA5 reanalysis (Hersbach et al., 2020), and hindcasts and forecasts from SEAS5. The variables we study are the zonal wind at 10 hPa 60°N, 2-meter temperature (T2), sea level pressure (SLP), and sea surface temperature (SST), all averaged over the extended winter season from December to March (DJFM).

The SEAS5 hindcasts and forecasts go back to 1981 and are initialized at the beginning of every month throughout the year. Each model run extends seven months into the future from initialization. As we study DJFM, we are able to use model runs that are initialized in early September (lead time 4–7 months), October (lead time 3–6 months), and November (lead time 2–5 months). We do not use December initializations, as the spread among the ensemble members for the DJFM period is quite narrow (especially for SST, given its slower evolution

than SLP and T2). For each of the hindcast dates between 1981 to 2016, there are 25 ensemble members. From 2017 to 2020, each of the forecasts have 51 ensemble members, but we only use the first 25 of these to have the same number of members per year for the entire 1981 to 2020 period. For each year we therefore have 75 ensemble members (25 members each for September, October, and November initializations), yielding a total of 3000 DJFM potential winters over the 40-year record (where we adopt the term 'potential' used by Spaeth and Birner (2021) to denote 'potential SSWs'). All initializations are treated equally in this analysis, without distinguishing with respect to lead time.

As a metric for vortex strength, we calculate the DJFM seasonal mean of zonally averaged zonal wind at 60°N and 10 hPa. We also compute seasonal means of the other variables, on a grid point basis. For most of the analysis, we use standardized values, where the standardization is based on seasonal climatological means and standard deviations. The unit is standard deviations (SD). The standardized version of the stratospheric winds is referred to as U10.

As the T2 and SST fields have substantial trends, we linearly detrend these data separately for each grid point. We do not detrend the other variables, as their trends have negligible impacts on the results.

We calculate an NAO index as the standardized principal component corresponding to the first Empirical Orthogonal Function (EOF) of SLP anomalies in the domain 20°N to 80°N and 90°W to 40°E. The EOFs are calculated separately for each data set using the *eofs* Python software package (Dawson, 2016), and the first EOF explains 54 and 44 percent of the DJFM SLP variance for ERA5 and SEAS5 data, respectively. The correlation between the NAO index and SLP and T2 is shown in Fig. A1.

Our Nino 3.4 index is calculated as the standardized area-weighted average of detrended SST anomalies between 5°S and 5°N and 170°E and 110°W. Another index is computed for each data set. We are interested in the pattern correlation between SST anomalies for a given sample and the typical SST anomalies associated with the NAO index in the North Atlantic. First, we compute the correlation between the NAO index and SST anomalies for each winter. This yields the maps shown in Fig. A2. Second, we multiply the SST anomalies in each grid point between 10°N and 65°N and between 80°W to 25°E by the correlations in Fig. A2, and then we compute the area-weighted mean for each winter. This yields an index of length 40 for ERA5 and an index of length 3000 for SEAS5. We define the standardized version of these as an 'NAO similarity' index. Positive values indicate that the SST anomaly pattern is consistent with a positive NAO index.

For the clustering analysis, we use the *k*-means (MacQueen, 1967) implementation in the Scikit-learn Python library (Pedregosa et al., 2011). The clustering was performed on detrended T2 anomalies over land for two regions: Eurasia (37°N to 75°N, 13°W to 175°E), and North America (30°N to 75°N, 165°W to 60°W). We also compute area-weighted detrended T2 anomalies for the same regions, using land points only.

3 Evaluating the model representation of the vortex and its surface signatures

First, we assess how the vortex strength in SEAS5 compares to that of ERA5. In Fig. 1, empirical cumulative distributions of the DJFM zonal-mean zonal wind component at 10 hPa, 60°N are shown for the two data sets. To check whether the differences can be explained by the

low number of samples in ERA5 (40), we generated 10,000 synthetic SEAS5 40-year time series by selecting a random ensemble member for each year of each time series. The shading spans the interval between the 2.5th and 97.5th percentile of the distributions of the synthetic SEAS5 time series. Focusing on DJFM, the zonal winds are generally stronger in ERA5 than in SEAS5, confirming earlier results from Portal et al. (2022). In the two middle quarters the differences are especially large, and the graphs for the individual winter months indicate that the largest differences occur in early winter (December and January), while the distributions in February and March are more similar in the two data sets. The weak vortex bias in SEAS5 is consistent with Monnin et al. (2022), who found that SEAS5 produced an average of 0.88 SSWs per winter between 1981 and 2019, compared with 0.71 SSWs per winter in ERA5.

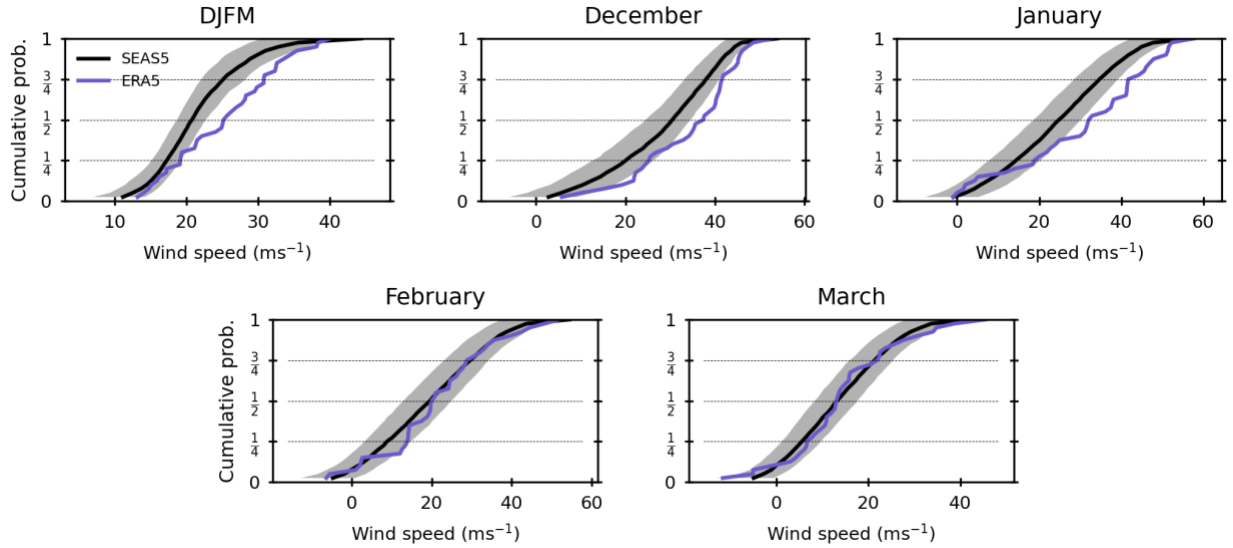

Figure 1. Empirical cumulative distribution functions (CDFs) of zonal means of 10-hPa zonal winds at 60°N for the winter mean (December–March; DJFM) and the individual winter months in ERA5 (blue) and SEAS5 (black). The shading shows the bootstrapped 95% confidence interval for SEAS5 (see text for details), and the dashed lines show the three quartiles which divide the data into four quarters.

In all the individual months and for the DJFM average, the sign of the skewness parameter of the two data sets is the same. The skewness in December is strongly and significantly negative (–0.56 in SEAS5 and –0.72 in ERA5). It is encouraging that the distributions match well in the lower and upper quarters (which are the focus of our study) despite the weaker zonal wind in SEAS5.

More important for the purposes of this study is that the near-surface temperature responses to anomalous vortex states in SEAS5 and ERA5 are comparable. To check that, we divide the data into four equal parts (quarters) based on U10. The quartiles – the boundaries between the quarters – are marked in Fig. 1, and the lower quartiles are 19 ms^{-1} (ERA5) and 17 ms^{-1} (SEAS5), while the upper quartiles are 31 ms^{-1} (ERA5) and 25 ms^{-1} (SEAS5).

The mean DJFM standardized 2-metre temperature (T2; detrended) and SLP anomalies corresponding to DJFM U10 values in the lower and upper quarters are shown for ERA5 in the

left column of Fig. 2. Note that these averages are based on only 10 winters in each quarter. In SEAS5, each quarter has 750 potential winters, and the averages in the lower and upper quarters are shown in the right column of Fig. 2.

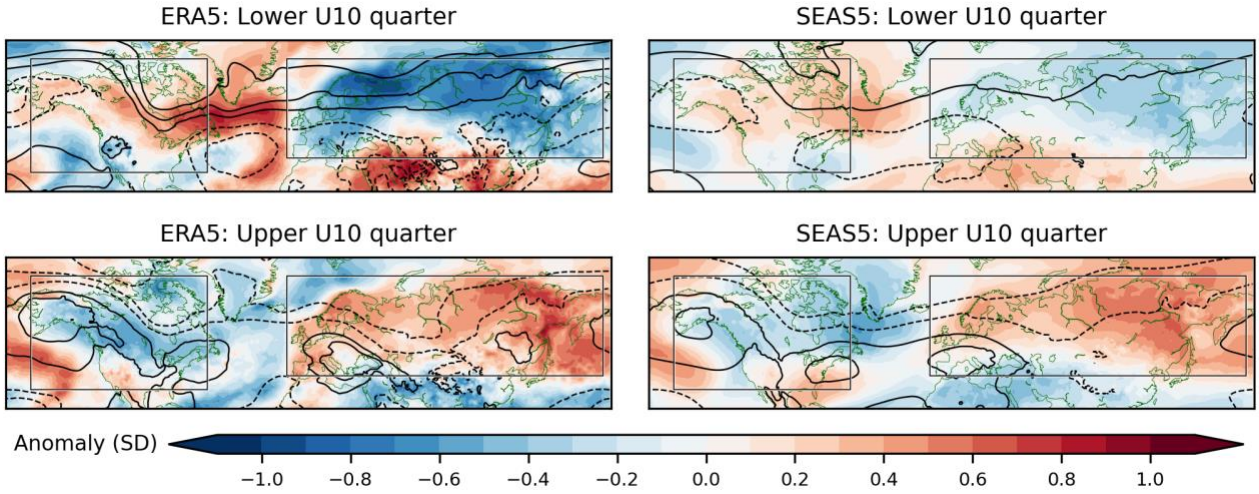

Figure 2. Mean DJFM T2 and SLP anomalies for the lower and upper U10 quarters in ERA5 (left column) and SEAS5 (right column), shown with colors and contours (every 0.25 SD), respectively. The black rectangles show the Eurasian and North American regions.

In the lower U10 quarter (the weak vortex cases), the T2 and SLP patterns in ERA5 are consistent with a negative NAO signature, both in terms of the classic SLP dipole over the North Atlantic and the corresponding T2 quadrupole (Hurrell, 1996; Stephenson & Pavan, 2003). Roughly opposite patterns are found in the upper quarter (the strong vortex cases).

Noting that the maximum magnitude of the mean surface anomalies in the lower quarter is considerably larger in ERA5 than in SEAS5, we check if this can be ascribed to sampling (since there are only 10 ERA5 samples in each quarter) by comparing area-weighted mean T2 in both data sets, for Eurasia and North America separately (using the regions outlined in the maps in Fig. 2). In Fig. 3, the orange histogram in each panel shows the full distribution of the 750 ensemble members in the lower and upper U10 quarters. These are not directly comparable to the mean ERA5 data, which only contains 40 data points (one for each year). To obtain a metric which is comparable, we create 10,000 synthetic 40-year time series based on SEAS5 data, where for each year we pull DJFM-mean U10, area-weighted T2 means, and the NAO index from a random ensemble member out of the 75 members available. Each member of the resulting 10,000 time series is then allocated to a U10 quarter, and for each subset (each consisting of 10 values), we compute the mean value of T2 and the NAO index. The interval between the 2.5th and 97.5th percentiles of these 10,000 values are shown with grey shading for each U10 quarter in Fig. 3. Because these intervals are based on averages of 10 values, the shaded intervals are considerably narrower than the full distribution of all the 750 values in each quarter (the orange bars).

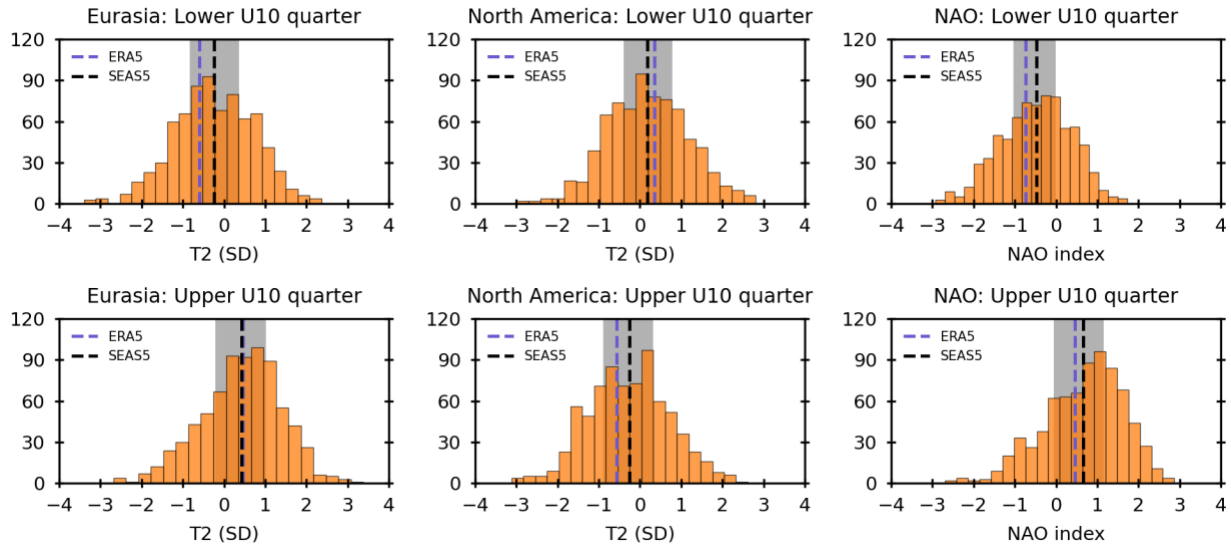

Figure 3. For area-weighted mean T2 in Eurasia (leftmost column) and North America (middle column), and for the NAO index (rightmost row), the orange bars show histograms (using 20 bins) of the 750 SEAS5 ensemble members in each quarter, the dashed blue line shows the quarter mean ERA5 value, the black dashed line shows the quarter mean for the 10,000 synthetic 40-year SEAS time series, and the shading shows the 95% confidence interval for SEAS5 (see text for details).

The top row of Fig. 3 shows that the mean Eurasian T2 anomaly in ERA5 is strongly negative (–0.6) for the lower U10 quarter, as reflected by the dominance of blue colors in the first panel of Fig. 2. The SEAS5 distribution has a mean value of –0.2 and a negative Eurasian T2 anomaly in 59% of the ensemble members. The ERA5 value is well inside the 95% SEAS5 interval (it corresponds to the 11th percentile of the SEAS5 values), so it cannot be ruled out that the ERA5 T2 anomaly is strongly negative due to small sampling. Another interpretation is that SEAS5 has a positive T2 bias in the lower U10 quarter because the model does not produce sufficiently cold conditions during weak vortex winters. Both interpretations may be true. In the upper U10 quarter, the mean Eurasian T2 anomaly in ERA5 (0.5) is practically identical to the mean SEAS5 value (0.4). In SEAS5, 70% of the ensemble members have a positive Eurasian T2 anomaly.

For the North American region (middle column of Fig. 3), the SEAS5 T2 distributions are shifted towards slightly warmer temperatures in the lower quarter (where 57% of the ensemble members are warm) and to colder temperatures in the upper quarter (where 59% of the members are cold), with mean values of 0.2 and –0.3 SD, respectively. These are opposite anomalies to those found for Eurasia, but similar in magnitude. The corresponding ERA5 mean values are twice as large (0.4 and –0.6, respectively), but these values are well inside the 95% interval of SEAS5.

In response to stratospheric vortex variability, the NAO index often shows a clearer signal than surface temperatures (Domeisen et al., 2020b). Hence, we now investigate the distribution of the NAO index in the lower and upper U10 quarters (rightmost column of Fig. 3). As mentioned previously, in reanalysis about two-thirds of SSWs are followed by dominantly

negative NAO conditions. In SEAS5, 69% of the ensemble members in the lower U10 quarter are NAO-negative, which corresponds well with the expected two-thirds frequency, suggesting this relationship holds on the seasonal-scale and even though the lower U10 quarter includes less extreme U10 values, not just SSWs. In the upper U10 quarter, 76% of the SEAS5 members are NAO-positive, and the ERA5 and SEAS5 mean values agree well. We note that the mean ERA5 NAO values in both U10 quarters are inside the 95% intervals for SEAS5 by solid margins.

On the continental scale for T2 and the NAO index, Fig. 3 shows that the ERA5 signatures are inside the range of natural variability in SEAS5. We interpret this as an indication that despite the stratospheric zonal wind biases that are evident in Fig. 1, the SEAS5 model produces realistic linkages between anomalous vortex states and surface weather patterns during DJFM.

Arguably the most interesting feature in Fig. 3 is the broad spectrum of each quarter of the SEAS5 data (orange histograms), which shows that the surface signatures have substantial seasonal-scale diversity. In the next section we investigate the diversity of the surface signatures in detail.

4 Diversity of the surface temperature response

The composite SEAS5 averages in Fig. 2 are based on a large number of ensemble members and therefore obscure the substantial variability evident in Fig. 3. To untangle this variance, we now look for clusters within the large number of ensemble members in the lower and upper quarters separately. As the middle quarters represent less extreme states and are overall closer to the climatological average, we do not consider them any further. The *k*-means cluster analysis (see Methods) is based on area-weighted T2 anomalies for land points only, and we study Eurasian and North American T2 responses separately. For practical purposes, we create three clusters for each combination of quarter and continent. Given that there is no objective choice of *k* in this case, we tested various options from two to six and concluded that three clusters give a representative picture of the diversity of surface signatures. Although differences in the population of each cluster could be taken as a measure of their relative likelihood (such as is the case with cluster-based weather regimes), we caution that there is insufficient evidence to support translating these statistics to real-world variability.

4.1 Eurasia

The top row of Fig. 4 shows the mean DJFM T2, SLP and SST anomalies in the three clusters based on the 750 cases in the lower U10 quarter. The clusters are named E-L1 to E-L3 (the letters ‘E’ and ‘L’ refer to ‘Eurasia’ and ‘Lower quarter’, respectively). Before we describe each cluster in detail, we summarize some key results upfront. The strongest surface anomalies in Eurasia occur when the state of the vortex and the SST anomaly pattern in the North Atlantic both influence the large-scale atmospheric flow in the same direction. A case in point is the E-L1 cluster, which has *both* a weak vortex *and* an SST pattern favorable for a negative NAO. We do not know if the SST pattern emerges as a response to the atmospheric flow or if it was pre-existing, but the pattern shown in Fig. 4 is in any case consistent with a feedback mechanism between the ocean and the atmosphere. The E-U3 cluster (where ‘U’ refers to ‘Upper quarter’) has a strong vortex in combination with an SST pattern that is highly favorable for a positive NAO. The result is a strong NAO signature and a clear corresponding quadrupole T2 signature. E-U1 also has a strong vortex, but the SST pattern is only weakly correlated with the typical

pattern associated with a positive NAO. Consequently, the resulting NAO index is weaker than the one in E-U3.

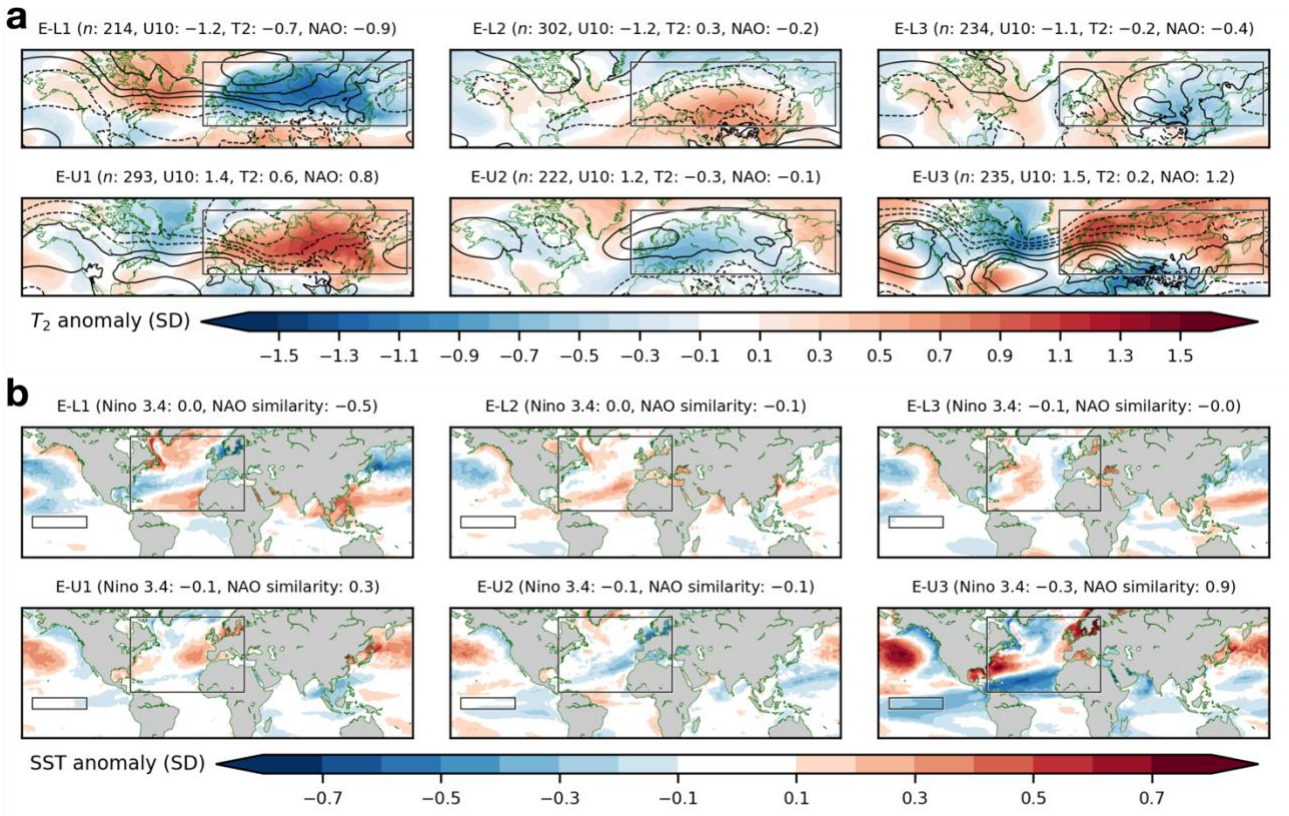

Figure 4. (a), Mean T2 anomalies (filled contours) and SLP anomalies (black contours every 0.25 SD, negative dashed, positive solid) for the Eurasian T2 clusters in the lower and upper quarters of U10. The black rectangle shows the boundaries of the Eurasian region, and the numbers in parentheses denote the number of members in each cluster, the mean U10 anomaly, the mean Eurasian T2 anomaly, and the NAO index in each cluster. (b), Mean SST anomalies for each cluster, with the mean Nino 3.4 and NAO similarity index values in parentheses (the black rectangles show the regions used to compute these indices). In all the panels, anomalies of magnitude greater than 0.1 SD (on average) are significant at the 5% level.

Recall that the average SEAS5 Eurasian T2 anomaly in the lower U10 quarter is –0.2 (Fig. 3). Yet, Fig. 4a shows that E-L1 is the *only* cluster in the lower U10 quarter that is clearly cold for most of the continent. All 214 members of E-L1 have a negative Eurasian T2 anomaly, indicating that the cluster captures continental-scale cold anomalies. SLP is anomalously positive over the high latitudes and negative over the midlatitudes. In other words, E-L1 conforms with the expected surface signature of a weak vortex winter. The mean SST anomaly in the E-L1 cluster in the North Atlantic (Fig. 4b) describes a tripole pattern typical of a negative NAO (see Fig. A2), and the NAO similarity index is –0.5.

The remaining two Eurasian clusters in the lower U10 quarter both have more members than E-L1, and their surface signatures are distinctly different. Although the mean NAO index in

E-L2 is negative, the Eurasian T2 anomaly is positive. A large majority (86%) of the cluster members are anomalously warm in Eurasia. The E-L3 cluster is composed of an east-west T2 dipole, with warm average conditions in the western part of the continent and cold conditions in the east. The NAO index is negative, but the spatial distribution of the SLP anomalies is quite different to those in E-L1. In contrast to E-L1, the SST signatures of E-L2 and E-L3 in the North Atlantic (Fig. 4b) bear little or no similarity to the typical NAO-negative pattern (Fig. A2), with near-zero mean NAO similarity index values. The lack of a favorable SST pattern in these clusters could be due to a lack of atmospheric forcing (because the NAO is insufficiently negative), but it is also possible that the NAO in E-L2 and E-L3 does not develop strongly negative conditions because the SST forcing is unfavorable. Possibly, both explanations are true. The fact remains that in E-L1, two factors which are known to influence the NAO index in a negative direction – a weak vortex and a favorable SST pattern in the North Atlantic – are present. In E-L2 and E-L3, only one of these factors is in place: a weak vortex.

The surface signatures associated with the strong vortex winters in the upper U10 quarter, shown in the bottom row of Fig. 4a, exhibit some symmetry with the signatures during the weak vortex winters. E-U1, the largest cluster, is essentially a mirror image of E-L1, with a strongly positive NAO index and a clearly positive average Eurasian T2 anomaly. All the ensemble members are anomalously warm in Eurasia. However, the NAO index is even more strongly positive in E-U3, but in that cluster the positive T2 anomaly is strongest in Northern Europe. E-U3 displays the classic quadrupole T2 pattern in the North Atlantic region. Its SST pattern (Fig. 4b) strongly resembles the pattern associated with a positive NAO (Fig. A2), with a mean NAO similarity index of 0.9. In contrast, the mean NAO similarity index of E-U1 is only 0.3. Of the six Eurasian clusters, E-U3 has the strongest link to ENSO, with a mean Nino 3.4 index of –0.3, suggesting that the cluster may be associated with the canonical stratospheric pathway of La Niña to the North Atlantic via a strengthening of the polar vortex (Iza et al., 2016). Interestingly, a mirror counterpart (with El Niño-like SSTs) is not apparent for the lower quarter U10 clusters (all three of which feature neutral ENSO conditions). E-U1 and E-U3 can be thought of as two different manifestations of a strong polar vortex/positive NAO, in which the strength of the positive temperature anomalies over Eurasia are related to where the high-latitude SLP anomalies are most negative. This effect is likely related to differences in the sign and amplitude of the pattern commonly described as Scandinavian blocking/anti-blocking (Ferranti et al., 2018; Kautz et al., 2022).

In E-U2, the T2 and SST patterns are the opposite of those for E-L2, and the NAO index is neutral. We note that the mean U10 (1.2) in E-U2 is 15–20 percent weaker than in E-U1 (1.4) and E-U3 (1.5), which may contribute to its damped NAO anomaly. As for the lower quarter, the expected surface signature associated with a strong vortex (positive NAO and warm conditions in Eurasia) is only in place when the SST pattern is favorable. These conditions occur in both E-U1 and E-U3.

4.2 North America

North America has not traditionally been seen as a region where surface impacts can be clearly linked to vortex anomalies (perhaps largely due to its position upstream of NAO variability). However, some recent extreme events and research have pointed to interesting linkages between the stratosphere and the troposphere over North America. We now investigate the clusters based on North American T2 anomalies, which are shown in Fig. 5. The weak vortex

clusters are named NA-L1 to NA-L3 (following the naming convention introduced for the Eurasian clusters), and the strong vortex clusters are named NA-U1 to NA-U3.

As might be expected given closer proximity and the known role of ENSO variability on the Pacific-North American region, in general the North American clusters have a stronger relationship with ENSO than the Eurasian clusters, with 4 of the 6 NA clusters associated with a substantial shift of the Nino 3.4 index. NA-L1 and NA-U3 are both associated with El Nino states in the tropical Pacific SSTs. NA-L3 and NA-U2 are both associated with La Nina states. However, our results highlight the modulating influence of the stratospheric vortex state on the teleconnection of ENSO to the North Atlantic-Eurasia region and the potential upstream influence on North America (Butler et al., 2014; Domeisen et al., 2019).

ENSO has a stratospheric pathway, which on seasonal timescales typically drives a weaker than normal vortex during El Nino, and vice versa during La Nina (Domeisen et al. 2019). This stratospheric pathway and its downward influence of the vortex then can either reinforce or dampen the NAO response to the ENSO tropospheric teleconnection (Polvani et al., 2017; Jiménez-Esteve & Domeisen, 2020). For example, NA-L1 shows a canonical Pacific-North American teleconnection during El Nino, with an anomalous Aleutian low, a trough over the southeastern US, and a ridge over Canada, while NA-U2 shows almost a mirror image associated with the canonical La Nina teleconnection (Butler et al., 2014; Domeisen et al., 2019). In both these clusters, the weaker (stronger) vortex reinforces the sign of the tropospheric teleconnection of ENSO to the negative (positive) NAO, respectively, leading to associated impacts over Europe. The SST pattern in NA-L1 overall corresponds to the pattern found in Dai and Hitchcock (2021) as a response to stratospheric forcing that tends to be associated with a weaker downstream response in the North Atlantic, as confirmed in Fig. 5a. On the other hand, NA-L3 and NA-U3 also have SST patterns indicative of significant ENSO forcing, but these clusters instead fall in vortex quarters which oppose the ENSO tropospheric teleconnection influence on the NAO. For example, NA-L3 occurs during a strong La Nina state but with a weak stratospheric vortex, so the influence of La Nina and the vortex essentially cancel out over the North Atlantic. Interestingly, the anomalies over northern North America are also much weaker, compared to NA-U2, where La Nina and the strong vortex act in concert, suggesting there is also an influence of the vortex on the upstream flow.

These results thus indicate the role of the vortex in modulating the expected ENSO teleconnection to the North Atlantic region, including its impacts on both downstream and upstream climate and associated seasonal-scale predictability.

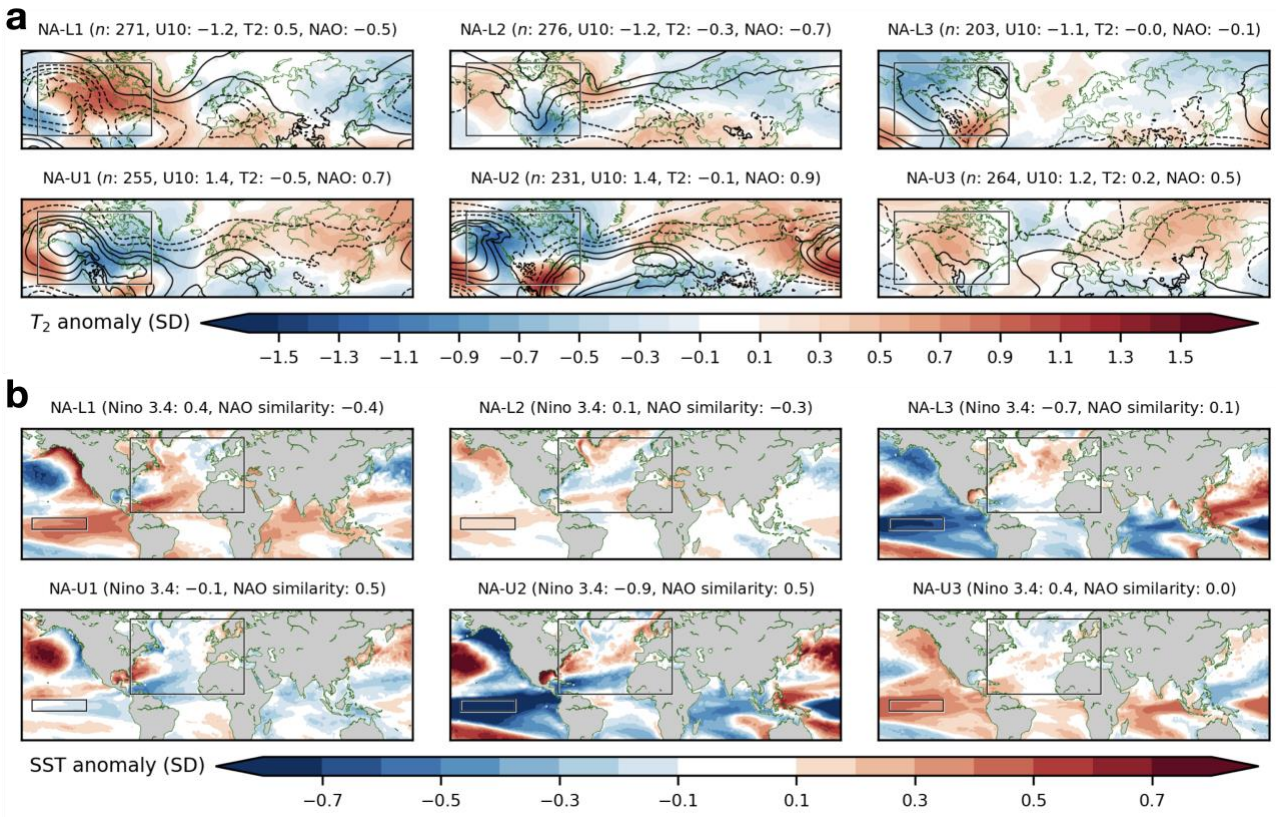

Figure 5. As Fig. 4, but for North America.

The two remaining North American clusters, NA-L2 and NA-U1, are nearly ENSO-neutral and thus represent the influence of the vortex on North American surface temperatures that occurs largely independently of ENSO. Although these patterns are based on opposing quarters of the polar vortex, both patterns are associated with cold over the North American region, though the regional spatial patterns are different. The weak vortex cluster NA-L2 shows an anomalous ridge stretching southward into the continent, a feature which is known to yield cold surges east of the Rockies (Colle & Mass, 1995). As a result, NA-L2 is 0.8 SD colder than NA-L1, with the main cold anomalies in the Contiguous US (CONUS), where 95% of the ensemble members have a negative area-weighted mean T2 anomaly. The strong vortex cluster NA-U1 is notably the coldest NA cluster, with strong advection of Arctic air associated with an extratropical SST pattern in the north-east Pacific resembling the so-called Pacific 'blob' and the SST anomalies during winter 2013/14, which drove a similar SLP and T2 anomaly pattern across North America (Hartmann, 2015; Liang et al., 2017). The anomalous high extending from Alaska along the west coast of North America, and the downstream cold anomalies, further resemble a pattern associated with downward wave reflection by the stratosphere (Messori et al., 2022; Millin et al., 2022), consistent with the strong U10 and the positive NAO downstream (Shaw & Perlwitz, 2013).

5 Summary and Discussion

Anomalous stratospheric polar vortex states are linked to weather events at the surface. However, the rarity of such events hampers our understanding of the full range of stratosphere–troposphere linkages. By using a large ensemble of model simulations, and by focusing on seasonal winter means, we filter out the impact of individual vortex events and elucidate the spectrum of possible persistent surface signatures. We are also able to link vortex and surface states to the oceanic background conditions, tying together two leading drivers and predictors of Northern Hemisphere seasonal climate. We do this separately for Eurasia and North America, which are influenced by stratospheric and oceanic variability in different ways.

By comparing the performance of the SEAS5 model to the ERA5 reanalysis, we show that the forecast model realistically reproduces vortex characteristics, as well as linkages between the vortex and surface weather. Although the average NAO index and Eurasian T2 anomaly associated with a weak vortex are more negative in ERA5 than in SEAS5, we show that both metrics in ERA5 are well within natural variability from the much larger sample size in SEAS5. This suggests that the strengths of the negative NAO and Eurasian T2 anomalies related to weak vortex events in the observed climate after 1980 could be higher than what is generally expected, perhaps simply because of the limited sample size in reanalysis with only 40 winters to study. Conversely, our results show that the NAO index and Eurasian T2 anomaly associated with strong vortex events are more positive in SEAS5 than in ERA5, suggesting that even more positive NAO and Eurasian T2 anomalies than those observed after 1980 are realistic. A cluster analysis performed on the SEAS5 ensemble members with the 25% weakest and strongest vortex winters yielded several notable results. Only one of the three weak vortex Eurasian clusters is clearly cold for most of the continent and has a strongly negative NAO index. This is qualitatively consistent with our finding that the mean Eurasian T2 anomaly during weak vortex winters is more negative in ERA5 than in SEAS5. We find that the Eurasian surface signatures are associated with North Atlantic SSTs as well as the state of the vortex. Though our approach makes it difficult to determine with certainty whether the SSTs are forcing or responding to the atmospheric anomalies, our results suggest that the atmosphere-ocean feedback is important for maintaining the persistence of the NAO signature. For example, in the coldest of the three Eurasian weak vortex clusters, the North Atlantic SST pattern is favorable for a negative NAO, while the SST pattern is neutral with respect to the NAO in the remaining two clusters. This shows that cold Eurasian conditions preferentially occur when there is a synergy between the oceanic conditions and the weak vortex state, extending results from Dai and Hitchcock (2021) for the North Pacific. Similarly, the North Atlantic SST patterns in the two strong vortex clusters with a clearly positive NAO are favorable for a positive NAO. In the strong vortex cluster with the most strongly positive NAO, the average Nino 3.4 index is negative, suggesting a role for a La Niña teleconnection consistent with previous studies (Iza et al., 2016; Polvani et al., 2017).

The linkage between tropical SSTs (e.g., ENSO) and the surface signature is more dominant in North America than in Eurasia. For both weak and strong vortex terciles, the clusters exhibit either an El Nino, ENSO-neutral, or La Nina state. For those clusters with active ENSO forcing, the ENSO tropospheric teleconnection is then either amplified or dampened by the downward influence of the vortex on the NAO. La Niña winters exhibit the expected T2 dipole over North America, with cold conditions in the northwest and warm conditions in the southeast US, but the T2 anomalies are substantially stronger when La Niña conditions coincide with a strong vortex and a positive NAO index than when the vortex is weak and the NAO is

491 negative. Similarly, El Niño winters are warm in the northwest US and cold in the southeast US,
492 but the T2 anomalies are stronger when the vortex is weak and the NAO is negative than when
493 the vortex is strong and the NAO is positive. The two remaining clusters with near-neutral ENSO
494 demonstrate the influence of the vortex on North America independently of ENSO. Interestingly,
495 for both the weak and strong vortex ENSO-neutral clusters the response is anomalously negative
496 for T2 over the entire North America region, though the patterns differ spatially. The regional
497 differences are dependent on exactly where the anomalous ridge sets up. Notably, the strong
498 vortex cluster is linked to strong ridging over the western US, which has previously been linked
499 on the sub-seasonal scale to wave reflection and associated cold air outbreaks over North
500 America (Messori et al., 2022; Millin et al., 2022).

501 Our key takeaway is that while weak vortex cases are often associated with cold
502 temperatures over Eurasia and North America, and vice versa for strong vortex cases, there are
503 also scenarios when instead the opposite is true. In fact, a relatively low proportion of the surface
504 impacts of weak vortex winters conform to the classic NAO-negative regime. Thus, the average
505 or 'canonical' surface signature related to seasonal-scale polar vortex variability – while robust –
506 disguises substantial variability which we cannot fully appreciate from the relatively small
507 observational sample size. Our results highlight the need for probabilistic predictions and a
508 nuanced analysis of confounding factors when using forecasts of the stratosphere for predicting
509 surface winter weather. Hence, decisions based on stratosphere–troposphere coupling, for
510 instance in the energy markets, can be improved by a greater understanding of this variability
511 and its relationship to concurrent SST patterns, with benefits to wider society (e.g., more reliable
512 consumer energy prices).

513 **Appendix**

514 As the NAO is a key component of the surface signatures, we show the correlation
515 between the NAO index and SLP and T2 in ERA5 and SEAS5 in Fig. A1. The correlation maps
516 are overall very similar, indicating that SEAS5 represents NAO variability well. However, we
517 note that there are some small differences. For SLP, the correlation pattern in the Atlantic is
518 slightly more zonally oriented in ERA5 than in SEAS5. One effect of this is that the positive
519 correlation for T2 in ERA5 is confined to the Eurasian continent, while in SEAS5 positive
520 correlations are also found in the Nordic Seas. The T2 correlation is also higher in Eurasia in
521 ERA5 – which means that NAO anomalies have a stronger effect on Eurasian T2 – than in
522 SEAS5.
523

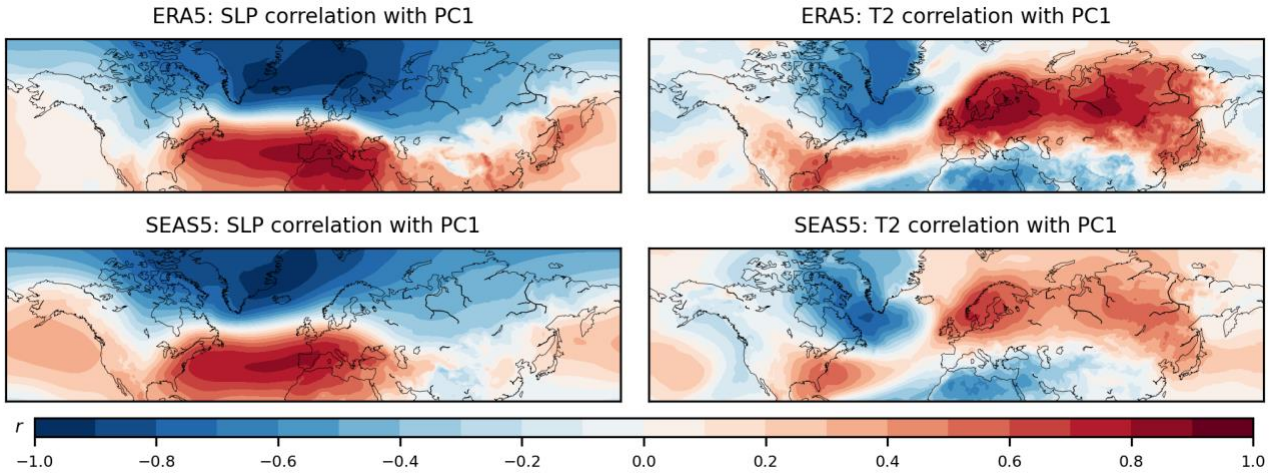

Figure A1. Correlation between the NAO index and, respectively, SLP (left) and T2 (right), based on all the 40 DJFM seasons in ERA5 (top row) and all the 3000 DJFM ensemble members in SEAS5 (bottom row).

We compare the relationship between the NAO index and SST in ERA5 and SEAS5 in Fig. A2. The correlation patterns for the two data sets are similar. In particular, the pattern in the North Atlantic is defined as a tripole which is known from many previous studies to describe the relationship between the NAO and SSTs (e.g., Rodwell et al., 1999; Czaja & Frankignoul, 2002; Cassou et al., 2007). There is also strong positive correlation in the North, Norwegian and Baltic Seas and somewhat weaker but significant positive correlation in the Northwest Pacific.

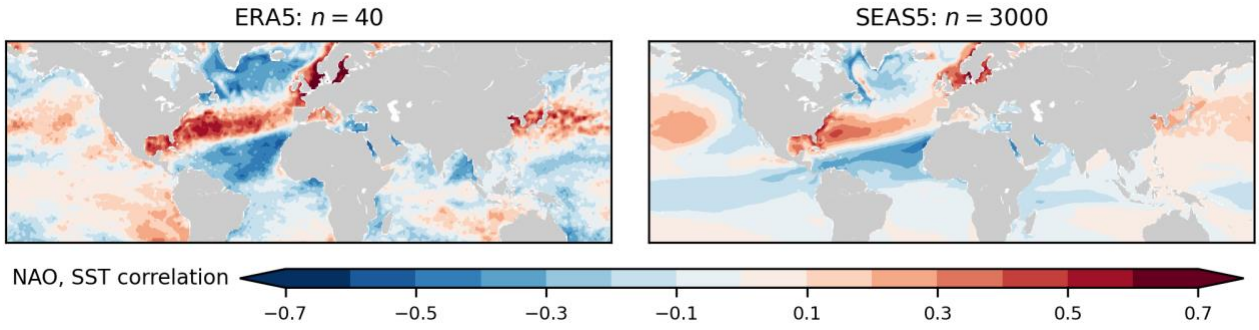

Figure A2. Correlation between the NAO index and (detrended) SSTs, based on all the 40 DJFM seasons in ERA5 (left) and all the 3000 DJFM ensemble members in SEAS5. Correlations of magnitude greater than 0.4 are significant at the 5% level for ERA5 (0.1 for SEAS5) data.

References

Afargan-Gerstman, H., & Domeisen, D. I. V. (2020). Pacific Modulation of the North Atlantic Storm Track Response to Sudden Stratospheric Warming Events. *Geophysical Research Letters, 47*(2), e2019GL085007. https://doi.org/10.1029/2019gl085007

Ambaum, M. H. P., & Hoskins, B. J. (2002). The NAO troposphere-stratosphere connection. *Journal of Climate, 15*(14), 1969-1978. https://doi.org/10.1175/1520-0442(2002)015<1969:TNTSC>2.0.CO;2

Ambaum, M. H. P., Hoskins, B. J., & Stephenson, D. B. (2001). Arctic Oscillation or North Atlantic Oscillation? *Journal of Climate*, *14*(16), 3495-3507. https://doi.org/10.1175/1520-0442(2001)014<3495:AOONAO>2.0.CO;2

Baldwin, M. P., Ayarzagüena, B., Birner, T., Butchart, N., Butler, A. H., Charlton-Perez, A. J., . . . Pedatella, N. M. (2021). Sudden Stratospheric Warmings. *Reviews of Geophysics*, *59*(1), e2020RG000708. https://doi.org/https://doi.org/10.1029/2020RG000708

Baldwin, M. P., & Dunkerton, T. J. (1999). Propagation of the Arctic Oscillation from the stratosphere to the troposphere. *Journal of Geophysical Research-Atmospheres*, *104*(D24), 30937–30946. https://doi.org/10.1029/1999JD900445

Baldwin, M. P., Stephenson, D. B., David W. J. Thompson, Dunkerton, T. J., Charlton, A. J., & O'Neill, A. (2003). Stratospheric Memory and Skill of Extended-Range Weather Forecasts. *Science*, *301*(5633), 636-640. https://doi.org/doi:10.1126/science.1087143

Barnes, E. A., Samarasinghe, S. M., Ebert-Uphoff, I., & Furtado, J. C. (2019). Tropospheric and Stratospheric Causal Pathways Between the MJO and NAO. *Journal of Geophysical Research: Atmospheres*, *124*(16), 9356-9371. https://doi.org/https://doi.org/10.1029/2019JD031024

Beerli, R., & Grams, C. M. (2019). Stratospheric modulation of the large-scale circulation in the Atlantic–European region and its implications for surface weather events. *Quarterly Journal of the Royal Meteorological Society*, *145*(725), 3732-3750. https://doi.org/https://doi.org/10.1002/qj.3653

Beerli, R., Wernli, H., & Grams, C. M. (2017). Does the lower stratosphere provide predictability for month-ahead wind electricity generation in Europe? *Quarterly Journal of the Royal Meteorological Society*, *143*(709), 3025-3036. https://doi.org/10.1002/qj.3158

Black, R. X., & McDaniel, B. A. (2004). Diagnostic Case Studies of the Northern Annular Mode. *Journal of Climate*, *17*(20), 3990-4004. https://doi.org/10.1175/1520-0442(2004)017<3990:DCSOTN>2.0.CO;2

Breivik, Ø., Aarnes, O. J., Bidlot, J.-R., Carrasco, A., & Saetra, Ø. (2013). Wave Extremes in the Northeast Atlantic from Ensemble Forecasts. *Journal of Climate*, *26*(19), 7525-7540. https://doi.org/10.1175/JCLI-D-12-00738.1

Brunner, M. I., & Slater, L. J. (2022). Extreme floods in Europe: going beyond observations using reforecast ensemble pooling. *Hydrol. Earth Syst. Sci.*, *26*(2), 469-482. https://doi.org/10.5194/hess-26-469-2022

Butler, A. H., Polvani, L. M., & Deser, C. (2014). Separating the stratospheric and tropospheric pathways of El Niño–Southern Oscillation teleconnections. *Environmental Research Letters*, *9*(2), 024014. https://doi.org/10.1088/1748-9326/9/2/024014

Butler, A. H., Sjoberg, J. P., Seidel, D. J., & Rosenlof, K. H. (2017). A sudden stratospheric warming compendium. *Earth Syst. Sci. Data*, *9*(1), 63-76. https://doi.org/10.5194/essd-9-63-2017

Cassou, C., Deser, C., & Alexander, M. A. (2007). Investigating the Impact of Reemerging Sea Surface Temperature Anomalies on the Winter Atmospheric Circulation over the North Atlantic. *Journal of Climate*, *20*(14), 3510-3526. https://doi.org/10.1175/JCLI4202.1

Charlton-Perez, A. J., Ferranti, L., & Lee, R. W. (2018). The influence of the stratospheric state on North Atlantic weather regimes. *Quarterly Journal of the Royal Meteorological Society*, *144*(713), 1140-1151. https://doi.org/10.1002/qj.3280

Chen, M., & Kumar, A. (2017). The utility of seasonal hindcast database for the analysis of climate variability: an example. *Climate Dynamics*, *48*(1), 265-279. https://doi.org/10.1007/s00382-016-3073-z

Cohen, J., Agel, L., Barlow, M., Garfinkel, C. I., & White, I. (2021). Linking Arctic variability and change with extreme winter weather in the United States. *Science*, *373*(6559), 1116-1121. https://doi.org/doi:10.1126/science.abi9167

Cohen, J., Foster, J., Barlow, M., Saito, K., & Jones, J. (2010). Winter 2009–2010: A case study of an extreme Arctic Oscillation event. *Geophysical Research Letters*, *37*(17), L17707. https://doi.org/10.1029/2010GL044256

Colle, B. A., & Mass, C. F. (1995). The Structure and Evolution of Cold Surges East of the Rocky Mountains. *Monthly Weather Review*, *123*(9), 2577-2610. https://doi.org/10.1175/1520-0493(1995)123<2577:TSAEOC>2.0.CO;2

Czaja, A., & Frankignoul, C. (2002). Observed Impact of Atlantic SST Anomalies on the North Atlantic Oscillation. *Journal of Climate*, *15*(6), 606–623. https://doi.org/10.1175/1520-0442(2002)015<0606:OIOASA>2.0.CO;2

Dai, Y., & Hitchcock, P. (2021). Understanding the Basin Asymmetry in Surface Response to Sudden Stratospheric Warmings from an Ocean–Atmosphere Coupled Perspective. *Journal of Climate*, *34*(21), 8683-8698. https://doi.org/10.1175/JCLI-D-21-0314.1

Dawson, A. (2016). eofs: A library for eof analysis of meteorological, oceanographic, and climate data. *Journal of Open Research Software, 4*(1). https://doi.org/10.5334/jors.122

Domeisen, D. I. V. (2019). Estimating the Frequency of Sudden Stratospheric Warming Events From Surface Observations of the North Atlantic Oscillation. *Journal of Geophysical Research: Atmospheres, 124*(6), 3180-3194. https://doi.org/10.1029/2018jd030077

Domeisen, D. I. V., Butler, A. H., Charlton-Perez, A. J., Ayarzagüena, B., Baldwin, M. P., Dunn-Sigouin, E., . . . Taguchi, M. (2020a). The Role of the Stratosphere in Subseasonal to Seasonal Prediction: 1. Predictability of the Stratosphere. *Journal of Geophysical Research: Atmospheres, 125*(2), e2019JD030920. https://doi.org/https://doi.org/10.1029/2019JD030920

Domeisen, D. I. V., Butler, A. H., Charlton-Perez, A. J., Ayarzagüena, B., Baldwin, M. P., Dunn-Sigouin, E., . . . Taguchi, M. (2020b). The Role of the Stratosphere in Subseasonal to Seasonal Prediction: 2. Predictability Arising From Stratosphere-Troposphere Coupling. *Journal of Geophysical Research: Atmospheres, 125*(2), e2019JD030923. https://doi.org/10.1029/2019jd030923

Domeisen, D. I. V., Garfinkel, C. I., & Butler, A. H. (2019). The Teleconnection of El Niño Southern Oscillation to the Stratosphere. *Reviews of Geophysics, 57*(1), 5-47. https://doi.org/https://doi.org/10.1029/2018RG000596

Domeisen, D. I. V., Grams, C. M., & Papritz, L. (2020c). The role of North Atlantic–European weather regimes in the surface impact of sudden stratospheric warming events. *Weather Clim. Dynam., 1*(2), 373-388. https://doi.org/10.5194/wcd-1-373-2020

Ferranti, L., Magnusson, L., Vitart, F., & Richardson, D. S. (2018). How far in advance can we predict changes in large-scale flow leading to severe cold conditions over Europe? *Quarterly Journal of the Royal Meteorological Society, 144*(715), 1788-1802. https://doi.org/https://doi.org/10.1002/qj.3341

Garfinkel, C. I., Waugh, D. W., & Gerber, E. P. (2013). The Effect of Tropospheric Jet Latitude on Coupling between the Stratospheric Polar Vortex and the Troposphere. *Journal of Climate, 26*(6), 2077-2095. https://doi.org/10.1175/JCLI-D-12-00301.1

Green, M. R., & Furtado, J. C. (2019). Evaluating the Joint Influence of the Madden-Julian Oscillation and the Stratospheric Polar Vortex on Weather Patterns in the Northern Hemisphere. *Journal of Geophysical Research: Atmospheres, 124*(22), 11693-11709. https://doi.org/https://doi.org/10.1029/2019JD030771

Greening, K., & Hodgson, A. (2019). Atmospheric analysis of the cold late February and early March 2018 over the UK. *Weather, 74*(3), 79-85. https://doi.org/https://doi.org/10.1002/wea.3467

Hartmann, D. L. (2015). Pacific sea surface temperature and the winter of 2014. *Geophysical Research Letters, 42*(6), 1894-1902. https://doi.org/https://doi.org/10.1002/2015GL063083

Hersbach, H., Bell, B., Berrisford, P., Hirahara, S., Horányi, A., Muñoz-Sabater, J., . . . Thépaut, J.-N. (2020). The ERA5 global reanalysis. *Quarterly Journal of the Royal Meteorological Society, 146*(730), 1999–2049. https://doi.org/10.1002/qj.3803

Hitchcock, P., & Simpson, I. R. (2014). The Downward Influence of Stratospheric Sudden Warmings. *Journal of the Atmospheric Sciences, 71*(10), 3856-3876. https://doi.org/10.1175/JAS-D-14-0012.1

Hurrell, J. W. (1996). Influence of variations in extratropical wintertime teleconnections on northern hemisphere temperature. *Geophysical Research Letters, 23*(6), 665-668. https://doi.org/https://doi.org/10.1029/96GL00459

Iza, M., Calvo, N., & Manzini, E. (2016). The Stratospheric Pathway of La Niña. *Journal of Climate, 29*(24), 8899-8914. https://doi.org/10.1175/JCLI-D-16-0230.1

Jiménez-Esteve, B., & Domeisen, D. I. V. (2020). Nonlinearity in the tropospheric pathway of ENSO to the North Atlantic. *Weather Clim. Dynam., 1*(1), 225-245. https://doi.org/10.5194/wcd-1-225-2020

Johnson, S. J., Stockdale, T. N., Ferranti, L., Balmaseda, M. A., Molteni, F., Magnusson, L., . . . Monge-Sanz, B. M. (2019). SEAS5: the new ECMWF seasonal forecast system. *Geosci. Model Dev., 12*(3), 1087-1117. https://doi.org/10.5194/gmd-12-1087-2019

Karpechko, A. Y., Hitchcock, P., Peters, D. H. W., & Schneidereit, A. (2017). Predictability of downward propagation of major sudden stratospheric warmings. *Quarterly Journal of the Royal Meteorological Society, 143*(704), 1459-1470. https://doi.org/10.1002/qj.3017

Kautz, L. A., Martius, O., Pfahl, S., Pinto, J. G., Ramos, A. M., Sousa, P. M., & Woollings, T. (2022). Atmospheric blocking and weather extremes over the Euro-Atlantic sector – a review. *Weather Clim. Dynam., 3*(1), 305-336. https://doi.org/10.5194/wcd-3-305-2022

Kelder, T., Müller, M., Slater, L. J., Marjoribanks, T. I., Wilby, R. L., Prudhomme, C., . . . Nipen, T. (2020). Using UNSEEN trends to detect decadal changes in 100-year precipitation extremes. *npj Climate and Atmospheric Science, 3*(1), 47. https://doi.org/10.1038/s41612-020-00149-4

Kent, C., Pope, E., Thompson, V., Lewis, K., Scaife, A. A., & Dunstone, N. (2017). Using climate model simulations to assess the current climate risk to maize production. *Environmental Research Letters*, *12*(5), 054012. https://doi.org/10.1088/1748-9326/aa6cb9

Kidston, J., Scaife, A. A., Hardiman, S. C., Mitchell, D. M., Butchart, N., Baldwin, M. P., & Gray, L. J. (2015). Stratospheric influence on tropospheric jet streams, storm tracks and surface weather. *Nature Geoscience*, *8*(6), 433-440. https://doi.org/10.1038/ngeo2424

Knight, J., Scaife, A., Bett, P. E., Collier, T., Dunstone, N., Gordon, M., . . . Walker, B. (2021). Predictability of European Winters 2017/2018 and 2018/2019: Contrasting influences from the Tropics and stratosphere. *Atmospheric Science Letters*, *22*(1), e1009. https://doi.org/https://doi.org/10.1002/asl.1009

Kolstad, E. W., & Charlton-Perez, A. J. (2011). Observed and simulated precursors of stratospheric polar vortex anomalies in the Northern Hemisphere. *Climate Dynamics*, *37*(7-8), 1443-1456.

Kretschmer, M., Cohen, J., Matthias, V., Runge, J., & Coumou, D. (2018). The different stratospheric influence on cold-extremes in Eurasia and North America. *npj Climate and Atmospheric Science*, *1*(1), 44. https://doi.org/10.1038/s41612-018-0054-4

Lawrence, Z. D., Perlwitz, J., Butler, A. H., Manney, G. L., Newman, P. A., Lee, S. H., & Nash, E. R. (2020). The Remarkably Strong Arctic Stratospheric Polar Vortex of Winter 2020: Links to Record-Breaking Arctic Oscillation and Ozone Loss. *Journal of Geophysical Research: Atmospheres*, *125*(22), e2020JD033271. https://doi.org/https://doi.org/10.1029/2020JD033271

Lee, S. H. (2021). The January 2021 sudden stratospheric warming. *Weather*, *76*(4), 135-136. https://doi.org/https://doi.org/10.1002/wea.3966

Lee, S. H., Charlton-Perez, A. J., Woolnough, S. J., & Furtado, J. C. (2022). How do stratospheric perturbations influence North American weather regime predictions? *Journal of Climate*, 1-56. https://doi.org/10.1175/JCLI-D-21-0413.1

Liang, Y.-C., Yu, J.-Y., Saltzman, E. S., & Wang, F. (2017). Linking the Tropical Northern Hemisphere Pattern to the Pacific Warm Blob and Atlantic Cold Blob. *Journal of Climate*, *30*(22), 9041-9057. https://doi.org/10.1175/JCLI-D-17-0149.1

Lü, Z., Li, F., Orsolini, Y. J., Gao, Y., & He, S. (2020). Understanding of European Cold Extremes, Sudden Stratospheric Warming, and Siberian Snow Accumulation in the Winter of 2017/18. *Journal of Climate*, *33*(2), 527-545. https://doi.org/10.1175/JCLI-D-18-0861.1

MacQueen, J. (1967). *Some methods for classification and analysis of multivariate observations.* Paper presented at the Proceedings of the fifth Berkeley symposium on mathematical statistics and probability.

Maycock, A. C., & Hitchcock, P. (2015). Do split and displacement sudden stratospheric warmings have different annular mode signatures? *Geophysical Research Letters*, *42*(24), 10,943-910,951. https://doi.org/https://doi.org/10.1002/2015GL066754

Messori, G., Kretschmer, M., Lee, S. H., & Matthias, V. (2022). Stratospheric Wave Reflection Events Modulate North American Weather Regimes and Cold Spells. *Weather Clim. Dynam. Discuss.*, *2022*, 1-29. https://doi.org/10.5194/wcd-2022-18

Millin, O. T., Furtado, J. C., & Basara, J. B. (2022). Characteristics, Evolution, and Formation of Cold Air Outbreaks in the Great Plains of the United States. *Journal of Climate*, *35*(14), 4585-4602. https://doi.org/10.1175/JCLI-D-21-0772.1

Monnin, E., Kretschmer, M., & Polichtchouk, I. (2022). The role of the timing of sudden stratospheric warmings for precipitation and temperature anomalies in Europe. *International Journal of Climatology*, *42*(6), 3448-3462. https://doi.org/https://doi.org/10.1002/joc.7426

Oehrlein, J., Polvani, L. M., Sun, L., & Deser, C. (2021). How Well Do We Know the Surface Impact of Sudden Stratospheric Warmings? *Geophysical Research Letters*, *48*(22), e2021GL095493. https://doi.org/https://doi.org/10.1029/2021GL095493

Pedregosa, F., Varoquaux, G., Gramfort, A., Michel, V., Thirion, B., Grisel, O., . . . Duchesnay, E. (2011). Scikit-learn: Machine Learning in Python. *Journal of Machine Learning Research*, *12*, 2825-2830.

Polvani, L. M., Sun, L., Butler, A. H., Richter, J. H., & Deser, C. (2017). Distinguishing Stratospheric Sudden Warmings from ENSO as Key Drivers of Wintertime Climate Variability over the North Atlantic and Eurasia. *Journal of Climate*, *30*(6), 1959-1969. https://doi.org/10.1175/JCLI-D-16-0277.1

Portal, A., Ruggieri, P., Palmeiro, F. M., García-Serrano, J., Domeisen, D. I. V., & Gualdi, S. (2022). Seasonal prediction of the boreal winter stratosphere. *Climate Dynamics*, *58*(7), 2109-2130. https://doi.org/10.1007/s00382-021-05787-9

Rodwell, M. J., Rowell, D. P., & Folland, C. K. (1999). Oceanic forcing of the wintertime North Atlantic Oscillation and European climate. *Nature*, *398*(6725), 320-323. https://doi.org/10.1038/18648

Rupp, P., Loeffel, S., Garny, H., Chen, X., Pinto, J. G., & Birner, T. (2022). Potential Links Between Tropospheric and Stratospheric Circulation Extremes During Early 2020. *Journal of Geophysical Research: Atmospheres*, *127*(3), e2021JD035667. https://doi.org/https://doi.org/10.1029/2021JD035667

Schubert, S. D., Chang, Y., DeAngelis, A. M., Koster, R. D., Lim, Y.-K., & Wang, H. (2022). Exceptional Warmth in the Northern Hemisphere during January–March of 2020: The Roles of Unforced and Forced Modes of Atmospheric Variability. *Journal of Climate*, *35*(8), 2565-2584. https://doi.org/10.1175/JCLI-D-21-0291.1

Shaw, T. A., & Perlwitz, J. (2013). The Life Cycle of Northern Hemisphere Downward Wave Coupling between the Stratosphere and Troposphere. *Journal of Climate*, *26*(5), 1745-1763. https://doi.org/10.1175/JCLI-D-12-00251.1

Spaeth, J., & Birner, T. (2021). Stratospheric Modulation of Arctic Oscillation Extremes as Represented by Extended-Range Ensemble Forecasts. *Weather Clim. Dynam. Discuss.*, *2021*, 1-25. https://doi.org/10.5194/wcd-2021-77

Stephenson, D. B., & Pavan, V. (2003). The North Atlantic Oscillation in coupled climate models: a CMIP1 evaluation. *Climate Dynamics*, *20*(4), 381-399.

Thompson, V., Dunstone, N. J., Scaife, A. A., Smith, D. M., Slingo, J. M., Brown, S., & Belcher, S. E. (2017). High risk of unprecedented UK rainfall in the current climate. *Nature Communications*, *8*(1), 107. https://doi.org/10.1038/s41467-017-00275-3

van den Brink, H. W., Können, G. P., Opsteegh, J. D., van Oldenborgh, G. J., & Burgers, G. (2004). Improving 104-year surge level estimates using data of the ECMWF seasonal prediction system. *Geophysical Research Letters*, *31*(17). https://doi.org/https://doi.org/10.1029/2004GL020610

van den Brink, H. W., Können, G. P., Opsteegh, J. D., van Oldenborgh, G. J., & Burgers, G. (2005). Estimating return periods of extreme events from ECMWF seasonal forecast ensembles. *International Journal of Climatology*, *25*(10), 1345-1354. https://doi.org/https://doi.org/10.1002/joc.1155

van der Wiel, K., Bloomfield, H. C., Lee, R. W., Stoop, L. P., Blackport, R., Screen, J. A., & Selten, F. M. (2019). The influence of weather regimes on European renewable energy production and demand. *Environmental Research Letters*, *14*(9), 094010. https://doi.org/10.1088/1748-9326/ab38d3

Wang, L., Hardiman, S. C., Bett, P. E., Comer, R. E., Kent, C., & Scaife, A. A. (2020). What chance of a sudden stratospheric warming in the southern hemisphere? *Environmental Research Letters*, *15*(10), 104038. https://doi.org/10.1088/1748-9326/aba8c1

Weaver, S. J., Kumar, A., & Chen, M. (2014). Recent increases in extreme temperature occurrence over land. *Geophysical Research Letters*, *41*(13), 4669-4675. https://doi.org/https://doi.org/10.1002/2014GL060300

White, I., Garfinkel, C. I., Gerber, E. P., Jucker, M., Aquila, V., & Oman, L. D. (2019). The Downward Influence of Sudden Stratospheric Warmings: Association with Tropospheric Precursors. *Journal of Climate*, *32*(1), 85-108. https://doi.org/10.1175/JCLI-D-18-0053.1